DOI: 10.1002/adma.201800273
Article type: Communication

3D DNA origami crystals

*Tao Zhang, Caroline Hartl, Kilian Frank, Amelie Heuer-Jungemann, Stefan Fischer, Philipp C. Nickels, Bert Nickel, Tim Liedl**

Faculty of Physics and Center for Nanoscience (CeNS), Ludwig-Maximilians-Universität, Geschwister-Scholl-Platz 1, 80539 München, Germany
E-mail: tim.liedl@physik.lmu.de

Keywords: DNA Origami crystals, gold nanoparticles, SAXS

3D crystals assembled entirely from DNA have been proposed and implemented with the declared goals to design materials on a molecular level and to arrange guest particles in predefined lattices. This requires design schemes that provide high rigidity and sufficiently large open guest space. We here present a DNA origami-based "tensegrity triangle" structure that assembles into a 3D rhombohedral crystalline lattice with an open structure in which 90% of the volume is empty space. Site-specific placement of gold nanoparticles within the lattice demonstrates that these crystals are spacious enough to efficiently host 20 nm particles in a cavity size of 1.83×10^5 nm^3, which would also suffice to accomodate ribosome-sized macromolecules. We validate the accurate assembly of the DNA origami lattice itself as well as the precise incorporation of gold particles by electron microscopy and small angle X-ray scattering (SAXS) experiments. Our results show that it is possible to create DNA building blocks that assemble into lattices with customized geometry. Site-specific hosting of nano objects in the optically transparent DNA lattice sets the stage for metamaterial and structural biology applications.

Engineering shape and interactions of nanoscopic building blocks allows for the assembly of rationally designed macroscopic three-dimensional (3D) materials with spatial accuracy inaccessible to top-down fabrication methods[1–3]. Owing to its sequence-specific interaction,

DNA self-assembly[4,5] allows the rational design of perfectly defined monomeric DNA nanostructures[6–8] and the precise tuning of monomer - monomer interaction strengths[8–10]. Polymerization of individual DNA motifs can result in designed macroscopic DNA crystals[3,11,12] and in large two dimensional templates that also have been employed for the 2D arrangement of guest molecules with high accuracy[13–19]. Additionally, DNA also serves as selective binder to connect metallic nanoparticles into highly ordered lattices[1,20–30] where the connectivity and structural stability of the network is provided by the inorganic core particles. We here show the assembly of a crystalline 3D lattice purely based on DNA origami[7,8] building blocks where the lattice geometry is fully determined by the origami monomer design. Note, this approach does not rely on metal colloids as linking units and in turn, the lattice is optically transparent (**Figure S1**) and only weakly scattering in the X-ray domain. We demonstrate that this type of construction allows for large unit cells and for the site-specific positioning of sizeable nano objects. Even though the first DNA crystals were demonstrated almost a decade ago[3,31,32], to date there have been no reports on pure 3D DNA crystals with units cells as large as the ones demonstrated here, suggesting that a "simple" scaling up of the unit cell size is not as trivial as it may seem at first glance and requires careful design, which will be discussed hereafter. There have been reports of 3D crystals with similar or larger unit cells made from other materials (e.g. block co-polymers[33]), however, these systems lack the ability of precise site-specific placement of guest molecules and modification – a feature that we introduce through the use of DNA origami.

For our purposes, the DNA origami building block must bear the following features: (i) high structural rigidity, (ii) polymerizability along three axes in space, and (iii) long edges to provide a large unit cell volume to host guest particles. Initially, we aimed at forming cubic lattices, however without noteworthy success. The corresponding DNA origami designs lacked both rotational symmetry and sufficient rigidity, which probably inhibited the growth of 3D lattices (**Figure S2**). Thus, inspired by earlier work by Chendge Mao and Nadrian

Seeman *et al.*[3,31,32], we built a large "tensegrity triangle" motif with DNA origami (**Figure 1**)[34]. This motif gains uniform rigidity from the intrinsic triangulation and its equally shaped three struts that are arranged in an over-under, over-under, over-under fashion. All of the three struts are 14-helix bundles (14HB) with a designed length of 67 nm and a diameter of ~ 12.5 nm. The three struts are folded from a single-stranded phage-derived scaffolding DNA (8634 nt) together with ~ 235 synthetic oligonucleotides in a temperature annealing ramp from 65 °C to 4 °C. Scaffold crossovers interconnect all struts in an over-under, fashion pre-determining the orientation of each bundle towards one another. One of the 14-helix bundles contains a "seam" where the scaffold strand does not continue through the entire bundle but is closed by oligonucleotides only (inset in **Figure 1**). By choosing identical cross section, axial orientation, and staggering of the three struts, the origami monomer can polymerize via blunt-end stacking into a rhombohedral lattice with the unit cell parameters $a = b = c = 67$ nm and $\alpha = \beta = \gamma = 106 \pm 4$ ° ($\neq$ 90 °, the three nucleotide long spacer between each of the 14 HB struts gives rise to flexibility at the joints and results in an uncertainty for the angles α, β and γ) (**Figure 1** and **Figure S3-S5**). **Figure S6** displays different views onto the unit cell of the rhombohedral lattice. Note that all three upper ends (blue) match all lower ends (orange) with similar interaction strength which enables the monomers to be incorporated into the crystal in three different orientations due to their three-fold rotational symmetry (**Figure 1B**).

First, the monomeric DNA origami structures were thermally annealed starting at 65 °C (for experimental details see **Materials and Methods**). To avoid kinetic trapping of the struts in an undesired conformation the oligonucleotides connecting the seam (**Figure S5**) were injected only midway through the folding process at 52 °C to improve the folding efficiency of monomers (**Figure S7**). The folded triangles were purified from excess oligonucleotides by PEG precipitation before analysis by transmission electron microscopy (TEM) imaging and polymerization (**Figure 2A**). Note that due to their structural similarity, misfolded structures

(**Figure 2A** asterisk) could not be removed from correctly folded structures during the purification step and thus remained in solution during crystal growth.

To initiate the growth of the 3D lattices, "polymerization strands" were added in a ten-fold molar excess over the purified monomers. These oligonucleotides completed the formation of each of the ends of the struts and thus established shape-complementary blunt ends. The sample mix was incubated at a constant temperature of 47 °C for 90 hours and then deposited and dried on TEM grids. TEM and SEM images of origami lattices show the surface-morphology of a regular, hexagonal pattern with a center-to-center spacing between the monomers of 64 nm, which deviates slightly from the designed strut length of of 67 nm and reflects the fact that helices in a DNA origami structure are not perfectly straight but undulate in a chicken-wire geometry effectively shortening the struts (**Figure 2B-F**). Close-up views display multiple layers of the lattice (**Figure 2E, Figure S8** and Figure **S9**). Due to the obtuse interaxial angle of the building blocks, the lateral extensions along the [111] plane exceeds those of all other planes. Consequently we predominantly observe hexagonal patterns corresponding to a top view perspective of the [111] plane (**Figure S10**). The magnified inset of the building blocks shown in **Figure 2B** confirms the correct chiral over-under orientation of the struts. Low magnification SEM images reveal the polycrystalline nature of lattice patches that are tens of micrometers in size with single domains spanning up to about 2.5 μm^2 (**Figure 2D** and **Figure S9b** & **9c**). Of particular interest is the observation that although defective triangles are present during the growth process, they seem to not incorporate themselves into the lattice patches but only appear in the periphery of the crystals (**Figure 2F**). We rationalize that, as the defective monomers lack the designed symmetry, their overall binding energy does not suffice to stabilize their integration into the lattice at the elevated temperatures during lattice growth. Correctly folded monomers, instead, can replace the defective ones, which permits the self-healing growth of the origami lattices. After growth and at ambient temperatures, however, defective monomers can bind to any border of the

lattice with just one or two connecting sites. Given the limited yield of correctly folded monomers, the observed assembly of macroscopic origami lattices indicates the effectiveness of the self-correcting processes and an overall robust lattice growth.

To demonstrate the precise placement of guest molecules in our origami lattices, we attached gold nanoparticles (AuNPs) of different sizes at the center of each triangular origami monomer (**Figure 3A**). This choice of position preserves the symmetry upon incorporation in the lattice and therefore maintains the rhombohedral lattice type. The particle-bearing building blocks were prepared and purified as described elsewhere[35]. Consecutive lattice growth occurred under equal conditions as for the pure DNA origami lattices. **Figure 3B** shows again the hexagonal pattern formed by origami triangles but this time with 10 nm or 20 nm AuNP groupings at the positions expected in this lattice orientation. As AuNPs are nearly vertically overlayed when looking down on the [111] plane, the number of nanoparticles per group actually indicates the number of origami layers in the lattice. Due to the strong electron scattering properties of the AuNPs, only a limited penetration depth into the dense samples can be achieved and perfect hexagonal patterns can be observed for not more than a few lattice layers (**Figure 3E** and **Figure S11 - S13**). A different type of nanoparticle pattern – rows of particles – emerged from adsorption of the same lattice in an orientation different from the [111] plane (**Figure 3C**), resulting in a different viewpoint. Low magnification TEM images illustrate the high quality of the particle-hosting lattices (**Figure 3D** and **Figure S13**). Note that there is no plasmonic coupling between AuNPs as the distance between the particles is too large (**Figure S1** and **S14**).

In order to access the full 3D crystal structure of our constructs in solution, we performed small angle X-ray scattering (SAXS) measurements on the triangular origami monomers, the pure origami lattices, and origami lattices hosting AuNPs. The X-ray intensities for all samples, extracted structure factors, and different model fits are shown in **Figure 4, Figure S15** and **Figure S16** and **Table S1**. All models are described in **note S1**.

From the scattering data of the monomeric DNA origami building block **(dataset i in Figure 4A)**, we obtain a strut length of $l = 64$ nm, strut radius of $r = 6.3$ nm, and an angle of $\alpha = 109°$ in very good agreement with the monomer design (**Figure S16a & b**)[36]. In the absence of "polymerization strands", the monomers are freely dispersed and we see no indication of assembly into any structure of higher order (**dataset i in Figure 4B**). This is very different for the origami crystals (**dataset ii in Figure 4A**) where pronounced Bragg peaks can be observed (a full list of identified Miller indices is given in **Table S2**). The intensity distribution of DNA origami lattices can be modeled by the product of the monomer form factor *P(q)*, and *S(q)*, the lattice structure factor[37]. In the fitting procedure, we allowed for variation of the interaxial angle, i.e. deformation of the monomer in the assembly process. The best fit confirmed that the monomer was not modified ($a = l = 65$ nm, $r = 6.3$ nm, $\alpha = 110$ °) and the resulting lattice is rhombohedral. The measured unit cell of our pure DNA lattice was found to have a volume of ~ 1.83×10^5 nm^3, which is about 100 times larger than that of previously reported pure DNA crystals[3] (**note S2**).

SAXS temperature studies revealed a sigmoidal curve, which is characteristic for cooperative effects and indicates the disintegration of the lattice at ~50°C, just above the temperature that we found to yield best crystal growth (**Figure 4C & D**). Interestingly, no expansion of the lattice appears prior to melting, i.e. the Bragg peak positions remain fixed until the peaks finally disappear, which is in accordance with our previous findings that DNA origami structures do not exhibit thermal expansion[36].

For DNA origami lattices hosting AuNPs, the crystal structures of the generated AuNP lattices are determined by the DNA origami lattice templates and the nanoparticle placement as described above. For both 10 nm and 20 nm AuNP lattices, the Bragg peaks resemble each other (vertical dashed lines in **Figure 4B datasets iii & iv**) indicating the same 3D lattice. SAXS intensities of Au–DNA lattices are dominated by the form factor of the AuNPs and contain their coherent diffraction (**Figure 4A datasets iii & iv**). Importantly, we observed a

precise correspondence between the unit cell parameters of pure origami and AuNP lattices, validating the experimental design of templated assembly in 3D by DNA frameworks.

Here we presented a route to building 3D lattices using designable DNA origami building blocks. Computationally identifying[38] and releasing strain in the structures could result in further improved monomer quality, which together with large-scale screening of crystallization conditions. e.g. with seeded growth or hanging/sitting droplet crystallization, will potentially lead to the formation of DNA origami single-crystals that can host a wide variety of components. Importantly, the use of rigid DNA origami building blocks permits the variable positioning of guest molecules, which would allow for different "guest lattices" within the same framework and even dynamically reconfigurable lattices. The size of our origami monomer and therefore of the lattice unit cell is primarily limited by the available length of scaffold strands, an obstacle that can be circumvented by employing, e.g., **λ** - phage scaffolds[39,40], hollow struts, monomers built up from hierarchical assembly[8] or by DNA brick-based assembly[41]. Combined with the optical transparency of the DNA frameworks, self-assembled metamaterials with precisely, 3D-arranged metamolecules become feasible which have potential applications as chiral media or Bragg reflectors. Furthermore, our DNA lattices are almost invisible under X-ray and electron irradiation, allowing for structural analysis of any incorporated guest molecule. With a view on proteins, their 3D arrangement could open up new paths to optical super resolution-based structure analysis and CryoEM tomography.[42]

Materials and Methods

Design and formation of DNA origami.

Design. The triangular origami was designed using caDNAno (design schematics in **Figure S3-S5**)[34]. The structure consists of three 14 helix bundles (14HBs) packed on a honeycomb lattice with a diameter of about 12.5 nm. These three 14HBs were designed to be

of the same length (199 bp) and display self-matching shape complementary blunt ends. The 14HBs were interconnected at selected positions by forced crossovers with three bases of scaffold spacers. In order to avoid topological traps of the struts in undesired geometries, a "seam" was introduced into one of the 14HBs. Here the scaffold does not run from one end of the strut to the other but loops back in the middle of the strut for each pair of helices (**Figure S5b**). The seam is closed by staple oligonucleotides. Groups of staple strands were divided into "connection" oligonucleotides (closing the seam), "polymerization" oligonucleotides (completing the ends of all struts and thus enabling blunt end stacking), "handle" oligonucleotides (for capturing the gold nanoparticles) and "core" oligonucleotides (all other strands). We observed that the presence of the seam oligonucleotides during the entire folding process leads to the formation of mainly deformed structures, possibly resulting from prematurely closed seams trapping the triangular struts in wrong geometries. Injection of the seam connectors at lower temperatures improved the yield of correctly folded triangles to ~ 60% (**Figure S7**). While all misfolded objects featured three edges, they did not exhibit the designed three-fold symmetry (**Figure 2A asterisk**). Note that due to their structural similarity to the targeted design, these defective objects could not be removed during the purification steps but remained in solution during crystal growth.

Folding and Purification. DNA origami structures were prepared by mixing core and handles staples (100 nM each, MWG Eurofins), and the circular DNA scaffold strand p8634 (12.5 nM, produced in house) in 1x TE-Mg^{2+} buffer (10 mM Tris, 1 mM EDTA, 18 mM $MgCl_2$). The mixture was thermally annealed from 65 °C to 4 °C over 35 h (15 min at 65 °C, cooling to 58 °C with a cooling rate of −1 °C per 5 min, 58 °C to 35 °C with rate of −1 °C per 1 h, and from 35 °C to 4 °C with rate of −1 °C per 5 min). Connection staples were injected into the folding mixture during the annealing process at 52 °C (**Figure S7**). Subsequently the folded DNA nanostructures were purified from excess DNA staples by agarose gel electrophoresis stained with 1x Sybr Safe (1 % agarose in 1x TAE 11 mM $MgCl_2$ buffer; 6.5 $V \cdot cm^{-1}$ for 2 h)

or by polyethylene glycol (PEG) precipitation[43,44]. For agarose gel purification, samples were run in 1 % agarose gels containing 1x Tris-acetate buffer (10 mM Tris, 10 mM acetic acid), 11 mM $MgCl_2$ and 1x SybrSafe (Thermo Fisher Scientific). All gels were cooled in ice water baths. Samples were separated at 6.5 $V \cdot cm^{-1}$ for 2 h following excision of the bands and recovery of the products by squeezing the band between two glass slides and collecting the resulting liquid droplet with a pipet. For PEG precipitation, equal volumes of 2x PEG buffer (15 % (w/v) PEG-8000, 2x TE, 500 mM NaCl, 20 mM Mg^{2+}) and unpurified folding solution were mixed and centrifuged for 30 min at 16,000 rcf. The resulting pellet was re-suspended in 1x TAE, 11 mM $MgCl_2$ buffer and subsequently shaken at 650 rpm, 30 °C for 24 h in order to re-disperse the origami structures.

Formation of DNA origami-gold nanoparticle conjugates.

Functionalization of gold nanoparticles with DNA. Gold nanoparticles (AuNPs, BBI International) of 10 nm, 20 nm and 30 nm (**Figure S13b** shows TEM images of the origami lattices hosting 30 nm AuNPs) were functionalized with 5'-thiolated 19T single-stranded DNA (Biomers) following published methods[35]. Briefly, TCEP (tris(2-carboxyethyl)phosphine) treated thiolated DNA was added in excess (200x molar excess for 10 nm AuNPs, 800x for 20 nm AuNPs, and 1800x for 30 nm AuNPs) to AuNPs. The mixture was incubated at room temperature for 24 hours before slowly increasing the salt concentration to 500 mM by addition of 1 M NaCl over a period of 6 h. DNA-modified gold nanoparticles were then purified using Amicon centrifugation filters (100K MW cut-off).

Conjugation of gold nanoparticles to DNA origami. Six staple oligonucleotides at the center of the triangular origami structure were extended from the struts with 19A bases serving as handles for attachment of the gold nanoparticles (one nanoparticle per origami nanostructure). An 8x molar excess of DNA-AuNPs was added to the DNA origami structures and incubated at room temperature overnight. The resulting DNA origami-gold nanoparticle conjugates were purified from excess gold nanoparticles in 1 % agarose gels containing 1x Tris-acetate,

11 mM $MgCl_2$ buffer, cooled in an ice-bath. Samples were separated at 7 $V \cdot cm^{-1}$ for 1.5 h. Bands were excised from the gel and recovered as described previously.

Polymerization of DNA origami into 3D lattices.

Polymerization. Polymerization oligonucleotides were mixed at 10x molar excess with purified bare triangular origami structures or with purified structures carrying gold nanoparticles. The buffer was then brought to 1x TAE and 15 mM $MgCl_2$. The polymerization mixture was incubated at a constant temperature of 47 °C for 3-4 days in a thermocycler. Owing to the different purification procedures and varying purification yields, the starting concentration of origami monomer for pure DNA origami lattice growth was ~ 25 nM (PEG purified), while for lattices with gold particles the starting concentration of the gold-carrying monomers ranged between 1 nM and 3 nM (gel purified).

As defective monomers lack the designed symmetry, their overall binding energy does not suffice to stabilize their integration in the lattice at the elevated temperatures during lattice growth.

Characterization techniques.

TEM. TEM imaging of DNA origami lattices was carried out using a JEM-1011 transmission electron microscope (JEOL) operating at 80 or 100 kV. For sample preparation 10 µL of polymerized DNA origami structures were deposited on glow-discharged TEM grids (formvar/carbon-coated, 300 mesh Cu; TED Pella, Inc; prod no. 01753 - f) for 1 h. For pure origami lattices and origami lattices containing 10 or 20 nm gold nanoparticles, grids were furthermore quickly washed once with 0.1 ‰ uranyl acetate solution (5 µL) and immediately afterwards stained with 0.1 ‰ uranyl acetate solution (5 µL) for 10 s. For origami lattices hosting 30 nm gold nanoparticles and the lattices for taking SEM images, grids were washed two times with water for 2 s.

SEM. The TEM grids were directly used for SEM imaging after 10 s sputtering using an Edwards Sputtercoater S150B 1990. The sputter target contained 60 % gold and 40 %

palladium. Process parameters used for sputtering were 7 mbar Ar, 1.1 kV, 35 mA. 10 s sputtering results in the deposition of layer of gold/palladium with a thickness of a few nm. The Au/Pd deposited TEM grids were directly fixed on the sample holder with carbon tape for SEM imaging with a Carl Zeiss LEO DSM 982 GEMINI (containing a source of thermal field emitting (TFE) cathode (1997) and a detector of LEO High Efficiency In-Lense Secondary Electrons). Beam parameters for taking imaging were set as 5 kV acceleration voltage and 30 µm aperture.

SAXS. The SAXS data were measured at four different sources. All sample to detector distances and beam centers were calibrated with silver behenate. The scattering data of the monomer shown in **Figure 4, dataset i** and **Figure S16a and b** was measured at an in-house X-ray source, which is described in detail in the literature [45]. The data of the undecorated DNA origami lattice and the DNA origami lattice decorated with 20 nm gold nanoparticles, **Figure 4, dataset ii and iii** and **Figure S15a** were measured at the SAXS beamline at ELETTRA in Trieste. The solutions of polymerized sample were loaded in a 1 mm flow-through quartz capillary and measured at 8 keV X-ray energy. A Dectris Pilatus 3 1M CMOS detector with 981 x 1043 pixels with 172 µm pixel size served as detector. The data of the DNA origami lattice decorated with 10 nm gold nanoparticles shown in **Figure 4, dataset iv** and the data of the DNA origami lattices shown in **Figure S15b and Figure S16 f,g,h,i** were measured at the beamline P08 at PETRA III (DESY) in Hamburg. A Perkin Elmer flat panel XRD 1621 with 2048 x 2048 pixels with 200 µm size served as detector. The solutions of polymerized sample were loaded in 2 mm quartz capillaries. The measurement was carried out at 20 keV in order to avoid radiation damage of the sample. The melting process shown in **Figure 4C** and **D** was recorded at the beamline ID02 of the European Synchrotron Research Facility (ESRF) in Grenoble at an X-ray energy of 12.46 keV. A Rayonix MX170-HS with 960x960 pixels of 177µm size served as detector. The sample was loaded in a temperature-controlled flow-through cell with a 1.5 mm quartz glass capillary.

Supporting Information
Supporting Information is available from the Wiley Online Library.

Acknowledgements
We thank Susanne Kempter for her help on TEM imaging and Philipp Altpeter on SEM imaging. We thank Martina Ober for her help with SAXS measurements during the beamtime at ESRF. We thank Alexander M. Maier, Iain MacPherson, and Florian Schüder for helpful discussions. We acknowledge support during beam time at DESY (P08, Uta Ruett),Elettra (Austrian SAXS, Heinz Amenitsch) and ESRF (ID02, Alessandro Mariani). This work was supported by the Deutsche Forschungsgemeinschaft through the SFB grant 1032 (TPA6 and A7), the Nanosystems Initiative Munich and the European Research Council grant agreement no. 336440 for ORCA (Optical Responses Controlled by DNA Assembly). This work benefitted from SasView software, originally developed by the DANSE project under NSF award DMR-0520547.

Received: ((will be filled in by the editorial staff))
Revised: ((will be filled in by the editorial staff))
Published online: ((will be filled in by the editorial staff))

References

[1] C. A. Mirkin, R. L. Letsinger, R. C. Mucic, J. J. Storhoff, *Nature* **1996**, *382*, 607.

[2] G. M. Whitesides, B. Grzybowski, *Science* **2002**, *295*, 2418.

[3] J. Zheng, J. J. Birktoft, Y. Chen, T. Wang, R. Sha, P. E. Constantinou, S. L. Ginell, C. Mao, N. C. Seeman, *Nature* **2009**, *461*, 74.

[4] N. C. Seeman, *Nature* **2003**, *421*, 427.

[5] N. C. Seeman, *J. Theor. Biol.* **1982**, *99*, 237.

[6] T. J. Fu, N. C. Seeman, *Biochemistry* **1993**, *32*, 3211.

[7] P. W. K. Rothemund, *Nature* **2006**, *440*, 297.

[8] S. M. Douglas, H. Dietz, T. Liedl, B. Högberg, F. Graf, W. M. Shih, *Nature* **2009**, *459*, 414.

[9] S. Woo, P. W. K. Rothemund, *Nat. Chem.* **2011**, *3*, 620.

[10] T. Gerling, K. F. Wagenbauer, A. M. Neuner, H. Dietz, *Science* **2015**, *347*, 1446.

[11] C. R. Simmons, F. Zhang, J. J. Birktoft, X. Qi, D. Han, Y. Liu, R. Sha, H. O. Abdallah,

C. Hernandez, Y. P. Ohayon, N. C. Seeman, H. Yan, *J. Am. Chem. Soc.* **2016**, *138*, 10047.

[12] E. Stahl, F. Praetorius, C. C. de Oliveira Mann, K.-P. Hopfner, H. Dietz, *ACS Nano* **2016**, *10*, 9156.

[13] E. Winfree, F. Liu, L. A. Wenzler, N. C. Seeman, *Nature* **1998**, *394*, 539.

[14] H. Yan, *Science* **2003**, *301*, 1882.

[15] J. Zheng, P. E. Constantinou, C. Micheel, A. P. Alivisatos, R. A. Kiehl, N. C. Seeman, *Nano Lett.* **2006**, *6*, 1502.

[16] W. Liu, H. Zhong, R. Wang, N. C. Seeman, *Angew. Chem. Int. Ed.* **2011**, *123*, 278.

[17] A. Aghebat Rafat, T. Pirzer, M. B. Scheible, A. Kostina, F. C. Simmel, *Angew. Chem. Int. Ed.* **2014**, *53*, 7665.

[18] Y. Ke, L. L. Ong, W. Sun, J. Song, M. Dong, W. M. Shih, P. Yin, *Nat. Chem.* **2014**, *6*, 994.

[19] P. Wang, S. Gaitanaros, S. Lee, M. Bathe, W. M. Shih, Y. Ke, *J. Am. Chem. Soc.* **2016**, *138*, 7733.

[20] A. P. Alivisatos, K. P. Johnsson, X. Peng, T. E. Wilson, C. J. Loweth, M. P. Bruchez Jr, P. G. Schultz, *Nature* **1996**, *382*, 609.

[21] D. Nykypanchuk, M. M. Maye, D. van der Lelie, O. Gang, *Nature* **2008**, *451*, 549.

[22] S. Y. Park, A. K. R. Lytton-Jean, B. Lee, S. Weigand, G. C. Schatz, C. A. Mirkin, *Nature* **2008**, *451*, 553.

[23] R. J. Macfarlane, B. Lee, M. R. Jones, N. Harris, G. C. Schatz, C. A. Mirkin, *Science* **2011**, *334*, 204.

[24] E. Auyeung, T. I. N. G. Li, A. J. Senesi, A. L. Schmucker, B. C. Pals, M. O. de La Cruz, C. A. Mirkin, *Nature* **2014**, *505*, 73.

[25] Y. Tian, T. Wang, W. Liu, H. L. Xin, H. Li, Y. Ke, W. M. Shih, O. Gang, *Nat. Nanotechnol.* **2015**, *10*, 637.

[26] Y. Tian, Y. Zhang, T. Wang, H. L. Xin, H. Li, O. Gang, *Nat. Mater.* **2016**, *15*, 654.

[27] W. Liu, M. Tagawa, H. L. Xin, T. Wang, H. Emamy, H. Li, K. G. Yager, F. W. Starr, A. V Tkachenko, O. Gang, *Science* **2016**, *351*, 582.

[28] M. R. Jones, N. C. Seeman, C. A. Mirkin, *Science* **2015**, *347*, 1260901.

[29] M. R. Jones, R. J. Macfarlane, B. Lee, J. Zhang, K. L. Young, A. J. Senesi, C. A. Mirkin, *Nat. Mater.* **2010**, *9*, 913.

[30] E. Auyeung, J. I. Cutler, R. J. Macfarlane, M. R. Jones, J. Wu, G. Liu, K. Zhang, K. D. Osberg, C. A. Mirkin, *Nat. Nanotechnol.* **2012**, *7*, 24.

[31] D. Liu, M. Wang, Z. Deng, R. Walulu, C. Mao, *J. Am. Chem. Soc.* **2004**, *126*, 2324.

[32] Y. Hao, M. Kristiansen, R. Sha, J. J. Birktoft, C. Hernandez, C. Mao, N. C. Seeman, *Nat. Chem.* **2017**, *9*, 824.

[33] Y. Zhao, K. Thorkelsson, A. J. Mastroianni, T. Schilling, J. M. Luther, B. J. Rancatore, K. Matsunaga, H. Jinnai, Y. Wu, D. Poulsen, J. M. J. Frechet, A. Paul Alivisatos, T. Xu, *Nat. Mater.* **2009**, *8*, 979.

[34] S. M. Douglas, A. H. Marblestone, S. Teerapittayanon, A. Vazquez, G. M. Church, W. M. Shih, *Nucleic Acids Res.* **2009**, *37*, 5001.

[35] R. Schreiber, J. Do, E.-M. Roller, T. Zhang, V. J. Schüller, P. C. Nickels, J. Feldmann, T. Liedl, *Nat. Nanotechnol.* **2014**, *9*, 74.

[36] S. Fischer, C. Hartl, K. Frank, J. O. Rädler, T. Liedl, B. Nickel, *Nano Lett.* **2016**, *16*, 4282.

[37] K. G. Yager, Y. Zhang, F. Lu, O. Gang, *J. Appl. Crystallogr.* **2014**, *47*, 118.

[38] J. Yoo, A. Aksimentiev, *Proc. Natl. Acad. Sci.* **2013**, *110*, 20099.

[39] P. C. Nickels, Y. Ke, R. Jungmann, D. M. Smith, M. Leichsenring, W. M. Shih, T. Liedl, B. Högberg, *Small* **n.d.**, *10*, 1765.

[40] A. N. Marchi, I. Saaem, B. N. Vogen, S. Brown, T. H. LaBean, *Nano Lett.* **2014**, *14*, 5740.

[41] L. L. Ong, N. Hanikel, O. K. Yaghi, C. Grun, M. T. Strauss, P. Bron, J. Lai-Kee-Him, F. Schueder, B. Wang, P. Wang, J. Y. Kishi, C. Myhrvold, A. Zhu, R. Jungmann, G. Bellot, Y. Ke, P. Yin, *Nature* **2017**, *552*, 72.

[42] T. G. Martin, T. A. M. Bharat, A. C. Joerger, X. Bai, F. Praetorius, A. R. Fersht, H. Dietz, S. H. W. Scheres, *Proc. Natl. Acad. Sci.* **2016**, *113*, E7456.

[43] S. M. Douglas, J. J. Chou, W. M. Shih, *Proc. Natl. Acad. Sci.* **2007**, *104*, 6644.

[44] E. Stahl, T. G. Martin, F. Praetorius, H. Dietz, *Angew. Chem. Int. Ed.* **2014**, *53*, 12735.

[45] L. K. Bruetzel, S. Fischer, A. Salditt, S. M. Sedlak, B. Nickel, J. Lipfert, *Rev. Sci. Instrum.* **2016**, *87*, 25103.

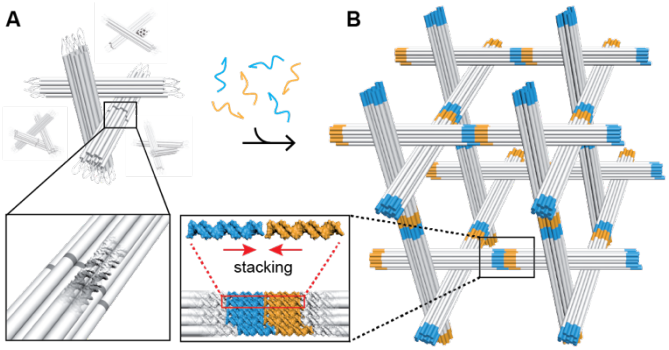

Figure 1. Schematic illustration of the triangular DNA origami building block design and assembly. **A**, The three 14-helix bundles of equal lengths are interconnected at defined positions and form a constrained triangular structure. A scaffold seam region is bridged by "connection" oligonucleotides (inset). **B**, Addition of oligonucleotides completing the struts results in the formation of self-matching shape complementary blunt ends. The three-fold symmetry facilitates the polymerization of the triangular monomers into a rhombohedral lattice via stacking interactions (inset). Details on the assembly process and additional 3D views are shown in **Figure S3** and **Figure S5**.

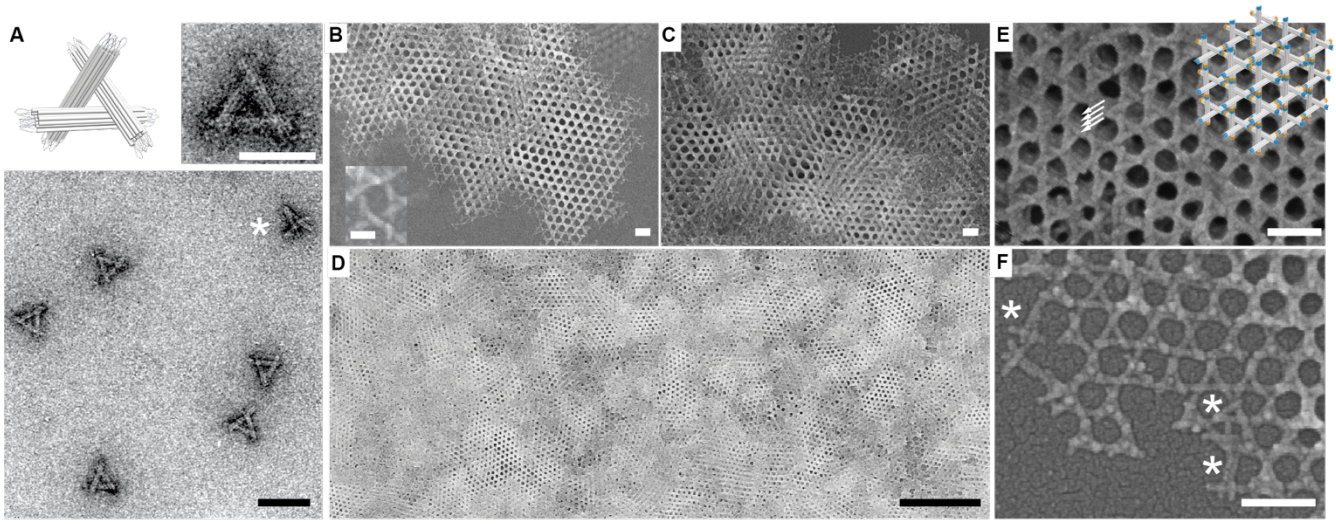

Figure 2. DNA origami lattices. **A,** TEM images of purified triangular DNA origami structures after purification and before addition of polymerization oligonucleotides that would initiate lattice growth. The asterisk points out a defective monomer. **B-F,** SEM images of DNA origami lattices. The inset in panel **B** exemplifies the left-handed over-under design. Panel **c** reveals the three-dimensionality of the assemblies and their polycrystallinity becomes apparent in the wide-field view shown in panel **D**. Although the lattices collapse on the imaging substrates during drying, the multiple layers and the original geometry can be inferred in a magnified view (white arrows, panel **E**). **F,** SEM image showing the border of a lattice with asterisks indicating defective monomers that were expelled from the lattice during the growth process and can only bind later at lower temperatures to the periphery. Scale bars in **A-F**: 100 nm, **D**: 1 µm, insets in **A** and **B**: 50 nm.

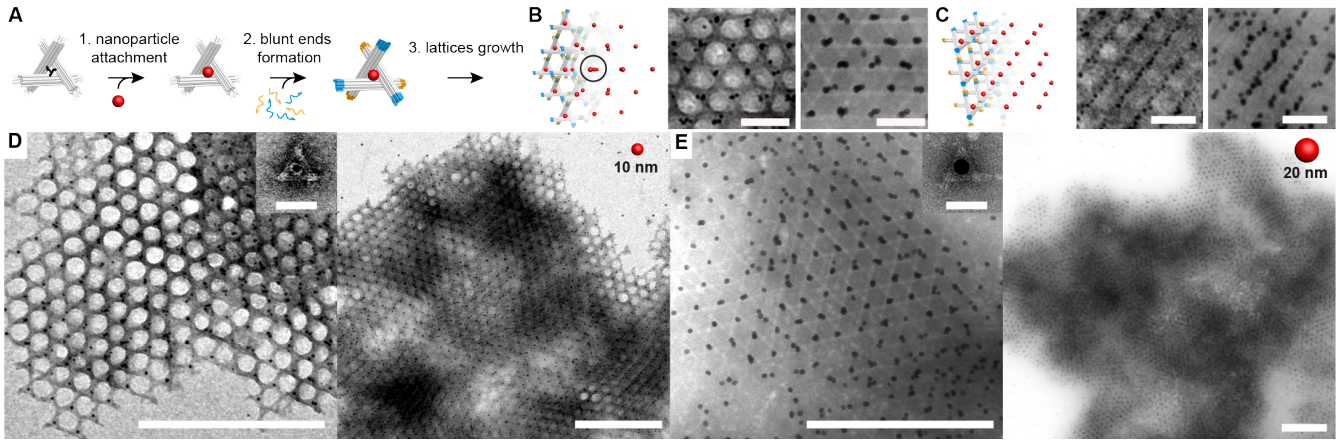

Figure 3. Hosting of gold nanoparticles in DNA origami lattices. **A,** Workflow to prepare gold nanoparticle lattices: 1) Folded and purified DNA origami triangles are incubated with gold particles overnight and then purified from excess particles. 2) Addition of the polymerization oligonucleotides to initiate the lattice growth process. 3) Incubation at 47°C for 3-4 days yields assembled host-guest lattices. **B, C,** Model views and TEM images of DNA origami lattice hosting 10 (left) or 20 nm (right) gold nanoparticles. The number of particles per grouping indicates the number of lattice layers overlapping at the respective points (black circle in **B**). **D, e,** Wide-field TEM images of origami lattices hosting 10 nm (**D**) and 20 nm (**E**) gold nanoparticles. Scale bars in **B** and **C**: 100 nm; **D** and **E** 500 nm, insets: 50 nm.

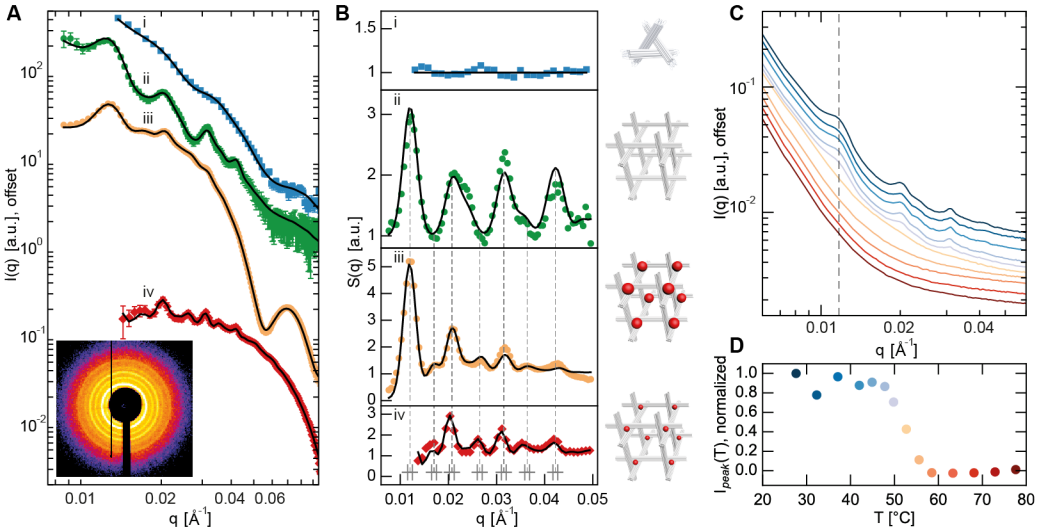

Figure 4. Small angle X-ray scattering (SAXS) measurements on the triangular origami monomers, pure origami lattices, lattices hosting gold nanoparticles and the in situ SAXS monitoring of lattice melting. A, SAXS intensities of triangular DNA origami monomers (i, blue), origami lattices (ii, green), and origami lattices hosting 20 nm (iii, orange) and 10 nm (iv, red) gold nanoparticles as a function of scattering vector q. Solid black lines: Model fits of total intensity. Inset: SAXS pattern of 10 nm gold-decorated sample. **B,** The monomer SAXS intensity (i, blue) divided by the fit yields a constant, indicating the absence of a lattice. Lattice structure factors from SAXS data (ii, green, iii, orange, iv red) Squared datapoints: in-house setup, dots: Elettra SAXS beamline, diamonds: DESY P08. Black lines: Model fits assuming a rhombohedral unit cell (parameters in the text). Vertical dashed lines label selected Bragg peaks found at the same position in all structure factors. The error range of the instrumental q resolution of each peak is $1 \cdot 10^{-3}$Å^{-1}. The differences in peak width and q range stem from the use of different beamlines (DESY P08 and Elettra SAXS). **C,** Scattering intensities of DNA origami lattices exposed to increasing temperatures (measured at ESRF ID02) show a sharp transition that indicates disintegration of the lattice at ~50°C. **D,** Plot of intensity of one peak vs. temperature. Data in A and C was scaled for clarity.